The semiconductor properties of passive films and corrosion behaviour of stainless steel reinforcing bars in simulated concrete pore solution

*I.G. Ogunsanya *, C.M. Hansson *+*

Mechanical and Mechatronics Engineering, University of Waterloo, Waterloo, ON, Canada N2L 3G1.

KEYWORDS: Stainless steel, carbon steel, concrete reinforcement, passive films, semiconductors, cement pore solution, chlorides.

*University of Waterloo, 200 University Avenue West, Waterloo, N2L 3G1.

+Corresponding author: 519-888-4538.

Email: (e-mail: chansson@uwaterloo.ca).

ABSTRACT

The vulnerability of concrete reinforcing steels to corrosion when depassivation occurs, typically in the presence of chloride, makes it important to understand the nature of the steels' passive films. In the Part I of the study, electrochemical techniques and Mott-Schottky analysis were used to investigate these films formed on five different grades of stainless steel and carbon steel reinforcing bars exposed to simulated concrete pore solution. The influence of the steel composition and surface finish on Mott-Schottky plots and the electronic properties are discussed in relation to the steels' corrosion resistance. A p-type semiconductor behaviour was observed in the stainless steel alloys in the cathodic potential regions and an n-type in the anodic potential regions. The n-type behaviour is similar to that observed in the carbon steel.

INTRODUCTION

The passive films formed on steel have been well studied in the literature using several techniques [1]–[9] such as in-situ Raman spectroscopy (RS), x-ray photoelectron spectroscopy (XPS), electron energy loss spectroscopy (EELS), electrochemical tunneling spectroscopy (ECT), electrochemical quartz crystal microbalance (EQCM), ellipsometry. Studies at the atomic structure level have described these films as extrinsic semiconductors [10]–[16]. Thus, it is expected that understanding the films' electronic behaviour can provide insight into the corrosion resistance of the steel. The Mott-Schottky (M-S) analysis [17], [18], which uses electrochemical impedance spectroscopy (EIS) to measure the film capacitance, has been used extensively to understand the electronic behaviour of the films formed on carbon steel [19]–[26], the traditional austenitic 316LN and 304L grades of stainless steel [5], [10]–[13], [27]–[30], and more recently, 2205 duplex stainless steel grade [31]–[33]. The potential difference across the semiconductor/electrolyte interface is the sum of those across the space charge layer of the semiconductor and the Helmholtz double layer in the electrolyte [16]. A series capacitor model is generally used to describe the capacitors present at the metal/electrolyte interface. However, the Helmholtz double layer capacitance is typically about 2-3 orders of magnitude greater than the space charge capacitance. Therefore, in the relationship applied to Mott-Schottky analysis,

Equation 1, the Helmholtz double layer component ($1/C_H$) becomes insignificant is normally omitted in studies of passive films [34].

The most commonly reported result from the M-S analysis is a plot of the inverse of the square of the capacitance of the passive film versus the applied potential, commonly called the Mott-Schottky plot. In addition to providing information on the capacitance of the film, the M-S analysis can reveal whether the semiconductor is p- or n-type and the defect density, N, of the film. Most studies have shown the passive film on iron-based alloys to be predominantly n-type, represented by Equations 2 [35], [36]. This M-S equation shows relationship between the capacitance of the space charge layer in the semiconducting passive film and applied electrode potential, E.

$$1/C^2=(1/C_{sc}^2 + 1/C_H^2) \qquad \textit{Equation 1}$$

$$1/C_{sc}^2 = \pm(2/\varepsilon\varepsilon_0 e N_A A^2)(E - E_{FB} - kT/e) \qquad \textit{Equation 2}$$

In this equation, C is the apparent capacitance, C_H is the capacitance of the Helmholtz double layer, C_{SC} is the capacitance of the space charge layer (i.e. interfacial capacitance) obtained from the relation C = 1/(-Z"2πf) [37], where Z" is imaginary part of the impedance and f is the frequency. A is the specimen area and ε and ε_0 are relative permittivities or (dielectric constants) of the semiconductor and of free space ($8.85\text{x}10^{-13}$ F/mm), respectively. E_{FB} is the flatband potential, the potential at which the semiconducting passive film is in equilibrium with its environment [38]. k = Boltzmann constant ($1.38\text{x}10^{-23}$ J/K); T = temperature (K) and e = charge of the electron ($1.602\text{x}10^{-19}$ C). N is the charge carrier density (N_D or N_A is the donor or acceptor density given by the slope (m) of the linear portion of the $1/C^2$ vs. E plot using the relation N = 2/є.ϵ_0.e.m [11]–[13]).

In addition, the film thickness, d, in nm, can be calculated [39]–[45] using the capacitance from the above analysis.

$$d = (\varepsilon\varepsilon_0 A/C) \qquad \textit{Equation 3.}$$

Where ε = 10 for carbon steel [20], [22], [46] and 15.6 for stainless steel [13], C is capacitance of the material calculated at different parts of the M-S plots (e.g. flatband potential (E_{FB}) and corrosion potential (E_{CORR})).

In most studies of the properties of the passive film, the physical meaning of the defect density, N, and flatband potential, E_{FB}, has not been well related to the corrosion behaviour of the material. Those studies correlating electronic properties of passive film with corrosion behaviour were either in non-ferrous materials [47], in very different solutions from that of this study [4], or in carbon steel [26] which is not main focus of this work. More recently, Cheng and co-workers [31]–[33] also related electronic properties of passive film to corrosion behaviour to observe the influence of ferrite and austenite phases in duplex stainless steel grades. Consequently, the overall goal of the present study has been to relate all the information obtained from the M-S analysis to the corrosion behaviour of the stainless steels determined by conventional electrochemical techniques. Moreover, most previous M-S tests on ferrous alloys have been performed on polished cross-sections of carbon steel [19]–[26] and stainless steel alloys (mostly, 316LN and 304L, and few recent studies of UNS S32205) [5], [10]–[13], [27]–[33] in an acidic, neutral or slightly alkaline environment. This environment is significantly different from that in concrete, for which the pH is typically > 13 [48].

The objectives of the present research were to analyse the semiconducting properties of the passive film formed on three austenitic and two duplex stainless steel grades of reinforcing bars (rebar) in the environments (pH and ionic concentrations) found in chloride-free and chloride-contaminated concrete and to relate these properties to the bars' corrosion behaviour in simulated concrete pore solution. The chloride levels investigated in this study were in the range found to initiate corrosion on stainless rebar in concrete [49]. The influence of surface condition on the semiconductor parameters was assessed by testing the polished cross-section as well as "as-received" bars. Measurements were also made on carbon steel rebar (also known as "black steel rebar") for comparison purposes.

MATERIALS AND METHODS

For application as concrete reinforcement, the surface of stainless reinforcing bars is sand blasted and acid-pickled after their hot rolling and heat treatment to remove the mill-scale and any chromium-depleted layer, respectively. The bars are heavily deformed with circumferential and longitudinal ribs and, consequently, it is anticipated that their surface films and corrosion behaviour would be highly non-uniform. Investigating the bars in this condition was aimed at determining the corrosion behaviour as it would occur in service.

The M-S tests and corrosion tests were carried out in "simulated concrete pore solution": a KOH+NaOH+$Ca(OH)_2$ mix corresponding to that obtained by pore solution expression from a 75% Portland cement+25% slag paste with a 0.40 water/cementitious materials ratio [50]. Chlorides were added to the solutions in the concentration range that has been reported to cause corrosion initiation on stainless rebar [49], [51]–[53].

The grades and chemical compositions of the steels are presented in Table 1.

Specimen preparation

All bars were ribbed obtained from a commercial supplier. The 304L bars had a 20 mm nominal diameter while all the other bars were 15 mm nominal diameter. For the specimens designated as 'as-received' bars, 125 mm lengths of each grade were prepared as follows. A hole was drilled at one end and a solid copper wire was soldered for an electrical connection. Lacquer was applied to both ends to cover the soldered connection and limit the exposed length to 76 mm, giving an exposed surface area of 3581 mm^2 (4780 mm^2 for the 304L). The bars were then cleaned with alcohol to remove oil and grease from handling and rinsed with distilled water. For the cross-section specimens, solid copper wires were soldered to 12.5 mm lengths of the bars which were then mounted in a silica fume mortar (2 parts sand, 1 part silica fume cement and 0.5 parts water). The exposed cross-sectional area was 177 mm^2 (314 mm^2 for the 304L). The specimens were then ground with increasing grit size up to 1200 and polished down to 1 µm with a diamond polish to achieve a consistent surface finish.

TABLE 1: Grades and composition of the bars from the mill certificate provided by the manufacturer.

Class	Rebar grade	In text as	Composition (wt.%)							
			Cr	Ni	Mo	Mn	Si	Cu	C	N
Austenitic	UNS S31653	316LN	17.60	9.50	2.01	1.10	0.70	0.40	0.03	0.14
	UNS S30403	304L	17.90	8.20	0.50	1.30	0.60	0.60	0.03	0.13
	UNS S24100	24100	17.10	0.90	0.19	12.12	0.70	0.14	0.04	0.34
Duplex	UNS S32205	2205	22.70	4.60	3.03	1.40	0.60	0.20	0.02	0.14
	UNS S32304	2304	22.40	3.92	0.20	1.80	0.60	0.30	0.02	0.14
Carbon steel	400W	Carbon	0.10	0.06	0.01	1.31	0.18	0.26	0.21	0.01

Experimental setup

For each type of specimen (as-received and cross-section), three replicate specimens from each grade were placed in cells with testing solution, shown in Table 2, for two weeks to allow them to reach equilibrium before any testing. The open circuit potentials, or corrosion potentials, E_{corr}, were monitored over this period. After initial testing, described below, chlorides were added as NaCl into each of the solutions weekly in 6% increments for the stainless steel grades and 0.6% increments for carbon steel by mass of pore solution. The maximum chloride contents were 21% and 2.4%, corresponding to pore solution contents in concrete with approximately 10.5% and 0.75% Cl^- by mass of cementitious material according to [50], [54].

TABLE 2: Testing solutions.

Composition (Molar)			pH
$Ca(OH)_2$	KOH	NaOH	
0.0014	0.48	0.13	~13.6

TABLE 3: Chlorides addition to testing solution.

	Chloride increment, Molar				
For stainless steel	0%	6%	12%	18%	21%
NaCl (M)	0	1.74	3.49	5.23	6.10
For carbon steel	0%	0.6%	1.2%	1.8%	2.4%
NaCl (M)	0	0.17	0.35	0.52	0.70

The specimens were tested in a three-electrode electrochemical cell with the steel specimens as the working electrodes (W.E), a saturated calomel reference electrode (R.E) and a mixed metal oxide-coated titanium mesh as counter electrode (C.E), as shown in Figure 1.

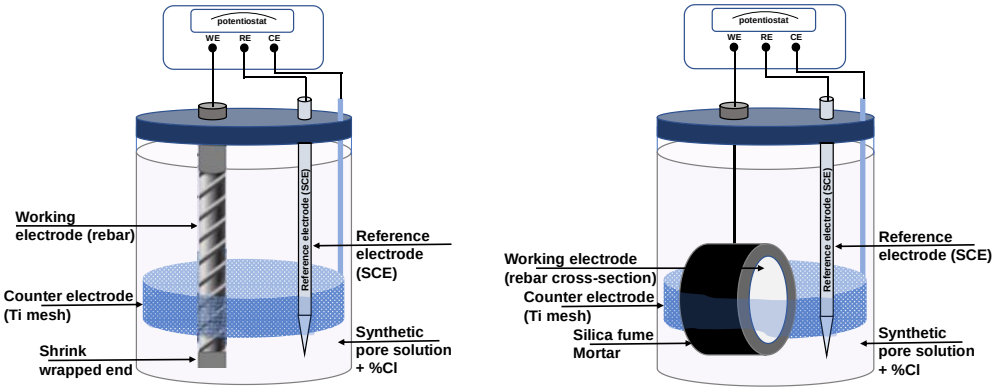

FIGURE 1. Test set-up for corrosion testing and Mott-Schottky analysis on as-received bars (left) and rebar cross-sections (right) [54].

Experimental methods

Using a BioLogic potentiostat, Model VSP, a potentiostatic linear polarization resistance (LPR) [55] and staircase potential electrochemical impedance spectroscopy (SPEIS) [37] were performed at every chloride level to determine the corrosion potential and current and the M-S behaviour, respectively. The potentiostatic LPR test consisted of the application of ±10 mV for 30 seconds and measurement of the steady state current at the end of the 30 s. The ratio of the applied potential to the measured current represent the Polarization resistance, R_P which was converted to corrosion current with the commonly used value for carbon steel rebar of 26 mV as the Stern-Geary constant. The constant values measured for stainless steel rebar [56] range from 20 to 28 mV. The SPEIS technique consists of a staircase potential sweep in which an impedance measurement (with desired frequency range) is conducted at each of a series of potential steps. The SPEIS was performed at 10 mV AC amplitude at frequencies from 100 – 1 kHz. The M-S plots presented in this paper were at 1 kHz, the maximum frequency at which the capacitance of the film was observed to be relatively unchanged [26]. 1kHz and a potential range of -1.5 – 0.6 V_{SCE} were also chosen to allow comparison with other results in the literature [11], [13].

One week after each chloride addition, an LPR was performed to detect the corrosion behaviour of the bar and, after a further 24 hours, the SPEIS test was conducted. After another 24 hours, chloride was increased in the solution and the film was allowed to attain equilibrium for a week before the next set of tests.

Using different specimens, taken from the same 1.2 m length of rebar, potentiodynamic cyclic polarization curves were obtained over the same potential range as the M-S tests in chloride-free and 6% chloride-containing solution.

RESULTS

An initial test was conducted to determine if it is possible to conduct multiple potential sweeps on the same sample without any adverse effect. This first part of the test was performed on two

separate “as-received” 2205 samples passivated in individual cells with chloride-free solution for two weeks. After passivation, NaCl was added to one of the cells at a concentration of 18% Cl^- and, after one week, the M-S tests were performed on both samples (Curve A – 0% Cl-, Curve B – 18% Cl^- in Figure 2). An M-S test was also performed on a passivated sample in solution without chlorides, Curve C, and again after 18% Cl^- addition, Curve D in Figure 2, which shows the M-S plots from these samples.

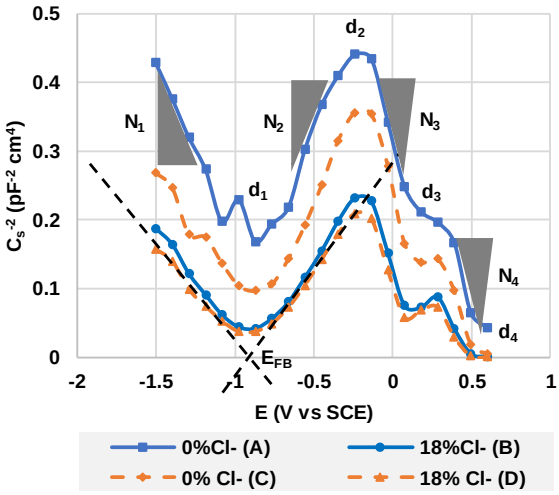

FIGURE 2. M-S plot conducted on 2205 samples in pore solution (PS) with and without chlorides. Curve A and B were obtained from two different bars tested in solution without and with chlorides respectively. Curve C and D were obtained from the same sample tested in solution before and after chlorides were added.

The curves with 0% Cl^- (Curves A and C) showed some variation which is attributed to the heterogenous surface of the bars. On the other hand, those plots for samples exposed to 18% Cl^- (Curves B and D) are very similar, suggesting that the influence of chlorides is greater than that of the surface inhomogeneities. The electronic properties of the passive films from this test, identified in Figure 2 and given in Table 4, are very similar, suggesting that multiple potential sweeps can be conducted on a specimen. These data cannot not be compared directly with those presented later in the paper because of the different exposed area of the 2205 bars employed in this preliminary test.

For corrosion measurements, the corrosion potential of three replicates of each steel grade was first monitored over a two-week period. Figure 3 shows the E_{CORR} values of one of the three

replicates of each grade. The E_{CORR} of all samples remained unchanged from day 8 to day 15, indicating that they reached steady state during that period.

TABLE 4: Electronic properties of curves identified in Figure 2. Linear regions and peaks where the defect densities (N_1 to N_4) and film thicknesses (d_1 to d_4) were calculated using Equations 2 and 3

M-S plots	Electronic properties								
	Acceptor density, N_1 (10^{21} cm^{-3}) -1.5 to -1	Donor density, N_2 (10^{21} cm^{-3}) -0.7 to -0.2	Acceptor density, N_3 (10^{21} cm^{-3}) -0.15 to 0.1	Acceptor density, N_4 (10^{21} cm^{-3}) 0.3 to 0.6	Flatband potential E_{FB} (V_{SCE})	Film at FB (-0.9 V) d_1 (nm)	Film at E_{CORR} (-0.2 V) d_2 (nm)	Film at 0.1 V d_3 (nm)	Film at 0.6 V d_4 (nm)
Curve A	6.21	5.30	2.85	4.27	-1.22	0.46	0.55	0.41	0.17
Curve B	8.79	7.30	3.49	6.72	-0.93	0.28	0.39	0.23	0.03
Curve C	8.06	5.10	2.83	4.27	-1.20	0.36	0.49	0.34	0.06
Curve D	10.51	8.00	3.70	7.26	-0.93	0.27	0.37	0.20	0.01

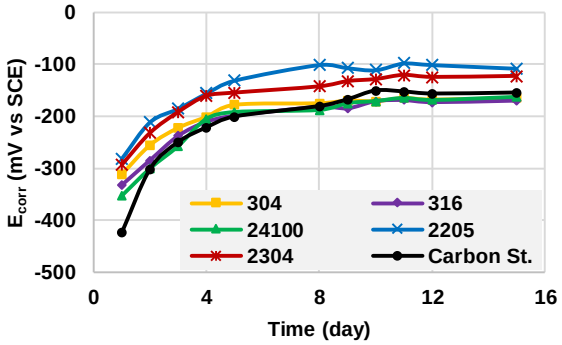

FIGURE 3. E_{CORR} values of bars in solution allowed to equilibrate for 2 weeks before any testing.

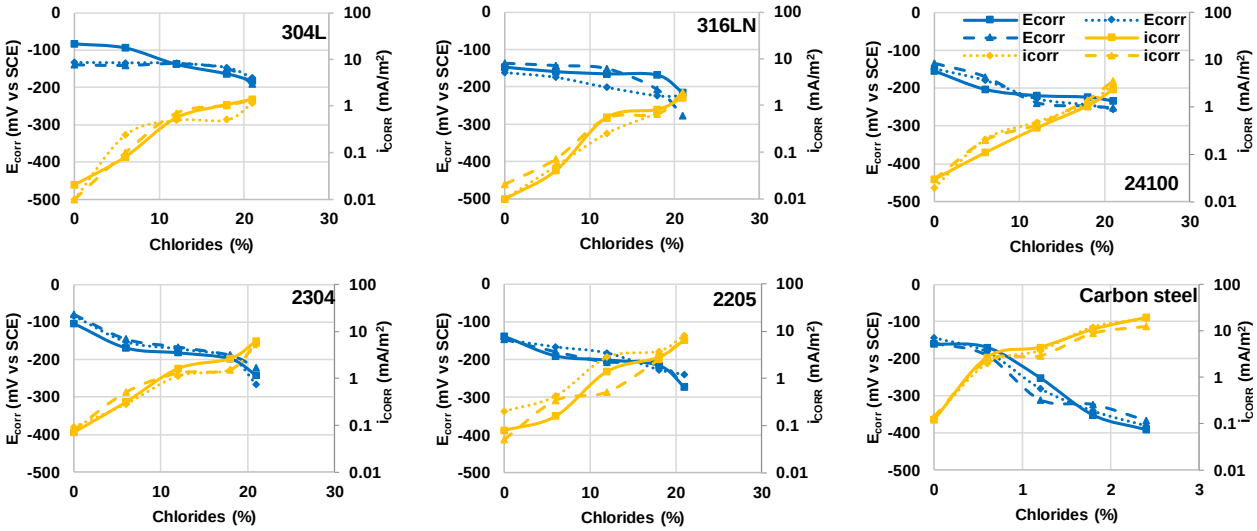

200

201 **FIGURE 4**. Corrosion potentials (blue) and current densities (yellow) obtained for three
202 replicates of each grade of "as-received" rebar in pore solution with increasing chlorides.

203 The corrosion potentials (E_{CORR}) and current densities (i_{CORR}) of the as-received bars in the pore
204 solution with increasing chlorides are presented in Figure 4. The i_{CORR} values of all bars increased
205 gradually with increasing chlorides, while their corresponding E_{CORR} values became gradually
206 more negative. This behaviour indicates that the ionic and electronic resistances of the passive
207 film was reduced by the chloride ions. The i_{CORR} values of the stainless steel and carbon steel in
208 solution with 21% and 2.4% chlorides, respectively, were between 1 - 10 mA/m^2 equivalent to
209 corrosion rates of between 1 - 10 µm/year. However, these values are the average over the whole
210 exposed area of the bar and it is highly likely that there are small areas of much higher corrosion
211 rates causing the more negative potentials. Consequently, it is not possible to determine a critical
212 chloride concentration for corrosion initiation from these data.

213 The Mott-Schottky plots in Figure 5 show the influence of increasing chlorides on one of three
214 replicates of each steel grade tested in their as-received conditions. A general observation for all
215 the stainless steel bars in chloride-free solutions, is the negative slope of the curves from -1.5
216 V_{SCE} to their flat band potential, a feature not observed in the curves for carbon steel.
217 Furthermore, on scanning the bars in solution in the anodic direction, both the stainless steels
218 and carbon steel displayed a positive slope n-type semiconductor passive film up to their
219 corrosion potentials (~ -0.15 V_{SCE}). At higher anodic potentials, the carbon steel showed a second
220 positive slope n-type semiconductor at potentials between -0.15 and 0.3 V_{SCE}, while the stainless

steel bars displayed a negative slope p-type semiconducting passive film at the same potential range. Both negative slopes are attributed to the presence alloying elements, particularly chromium These findings are in agreement with others' observations [5], [10]–[13], [27]–[33].

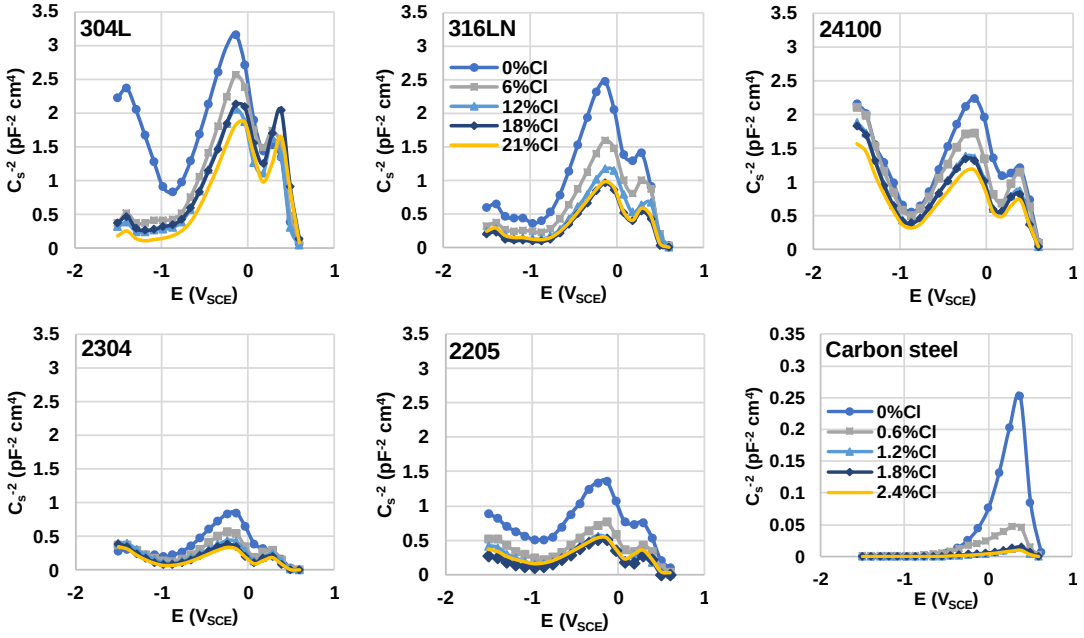

FIGURE 5. Mott-Schottky plot of the austenitic and duplex steels tested in the pore solutions with increasing chloride. Note the order of magnitude lower $1/C^2$ value for carbon steel.

The space charge capacitance, C, increases (shown in Figure 5 as decreasing $1/C^2$) with increasing chlorides. Since there is a direct relation between C and defect density, N, and, an inverse relationship with film thickness, d, these plots indicate an increase in defect density and decrease in film thickness with increasing chlorides in solution. This trend indicates that the passive film structure is increasingly unstable with increasing chloride concentrations, which agrees with the E_{CORR} and i_{CORR} data in Figures 4. The difference in capacitance between specimens in chloride-free solution and in solutions containing 6% Cl- (0.6% Cl-) is much greater than that between 6% Cl- (0.6% Cl-) and higher chloride levels. The increasing C values with chlorides is similar to those observed by [26] in similar solution pH and composition.

Figures 6A and 6B present the M-S plots obtained from three replicates of polished cross-sections of the 2205 bars tested in the solutions without chlorides and with 21% Cl-, respectively. Figures 6C and 6D are those obtained from testing the as-received bars in similar solutions, respectively and are presented here for easy comparison. Since there is good reproducibility in the M-S

behaviour of the polished surfaces, the electronic properties obtained from only one sample of each stainless steel alloy are presented in Table 11. A general observation is that the *shape* of the M-S curves is not affected by the surface finish of the bars, but the *scale* of the $1/C^2$ axis is shown to be different. Another observation from Figure 6 is that the M-S plots of the as-received bars are not as reproducible as those of the polished surfaces, but, the effect of chlorides on both surface conditions is similar.

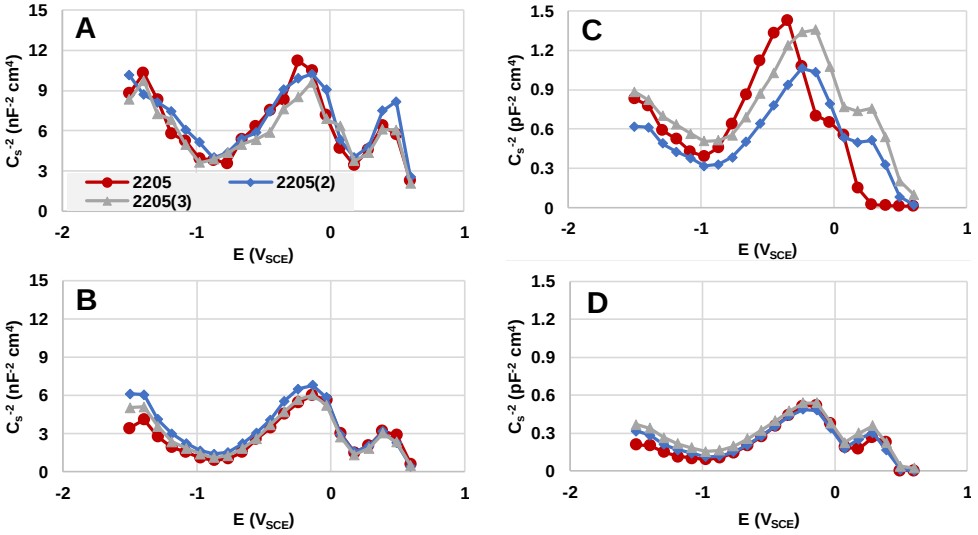

FIGURE 6. Mott-Schottky plots of three replicates of the 2205 stainless steel polished cross-sections (A and B) and as-received bars (C and D) bar tested in pore solution with 0% (A and C) and 21% (B and D) chlorides. The electronic properties are shown in Table 8.

DISCUSSION

The test performed to determine if repeated potential sweeps can be applied on the same steel specimens confirms the reproducibility of the results. Feng et al. [28] also repeated potential sweep on the same specimens and found no outliers in their result. Williamson and Isgor [26] found only slight differences in electronic properties obtained from repeated potential sweep on the same specimen and those from single potential sweep applied on a specimen. It is worth noting that in their test, potentials were applied at different passivation times (from 0.5 hours to 10 days) and not at different chloride additions as employed in this paper. In the current project, the bars were allowed to reach steady state before any application of potential sweeps, both initially and after each chloride addition.

Tables 5 to 10 summarise the electronic and electrochemical properties of three replicates of each grade of the as-received steels tested in pore solution. Table 11 presents the corresponding data for the polished cross-sections of the stainless steel bars. These tables provide the corrosion current density (i_{CORR}) and corrosion potentials (E_{CORR}) from LPR measurements; the flatband potential (E_{FB}), defect densities (N_1, N_2, N_3, N_4) and film thicknesses (d_1, d_2, d_3, d_4) at capacitance values corresponding to those shown in Figure 2. The 24100 bar was not tested at 18% Cl- due to power problem at the university.

These data are discussed below in terms of the influence of increasing chlorides in the pore solution, the rebar composition and the surface finish. A comparison of the defect densities, flatband potential, and film thicknesses, shown in Tables 5, 6, 9 and 10 with those from the literature shows that they are similar to those reported for 304L, 316LN and 2205 stainless steel alloys [5], [10]–[13], [27]–[33] and carbon steel [19]–[25], despite their different test solution concentration and pH. No references were found for the electronic properties of the 24100 and 2304 grades.

In chloride-free pore solution, the i_{CORR} values presented in Table 11 for the polished cross-sections of the bars were an order of magnitude lower than those tested in the as-received conditions, shown in Tables 5 - 9. However, after the addition of chlorides, the potentials and current densities in the two sets of specimens were similar. As indicated in Figure 2, the first negative slope in the M-S plots was used to calculate the N_1 values (the p-type, Cr-rich layer), while the next positive and negative slopes were used to calculate the values of N_2 (the n-type, Fe-rich layer) and N_3 (the p-type outer spinel layer) respectively.

Influence of increasing chlorides in the testing solution on electronic properties

Figure 7 shows that the defect densities (N_1 and N_2) increased with increasing chloride concentration, while film thicknesses (d_1 and d_2) decreased. This is in agreement with the decreasing (more negative) E_{CORR} and increasing i_{CORR} values with chlorides shown in Figures 4. It is reasonable that a passive film attacked by chlorides has a higher density of defects, indicating the non-stoichiometry of the space charge layer of the passive film. A high defect density is closely associated with a high probability of passivity breakdown since defects are potential sites

288 **TABLE 5**: Corrosion and film semiconductor data for as-received 304L bars tested in pore
289 solution, with the N_x and d_x values defined in Figure 2.

Chloride addition		Electronic properties										
		i_{CORR} (mA/m^2)	E_{CORR} (mV$_{SCE}$)	E_{FB} (mV$_{SCE}$)	N_1 (10^{21} cm^{-3})	N_2 (10^{21} cm^{-3})	N_3 (10^{21} cm^{-3})	N_4 (10^{21} cm^{-3})	d_1 (nm)	d_2 (nm)	d_3 (nm)	d_4 (nm)
0%	**1**	0.02	-83	-1020	1.13	1.10	0.65	0.65	0.55	0.75	0.76	0.18
	2	0.01	-133	-1030	1.08	1.27	0.84	0.90	0.49	0.67	0.66	0.22
	3	0.01	-139	-990	1.52	1.77	1.03	1.42	0.40	0.55	0.48	0.12
6%	**1**	0.08	-94	-910	2.68	1.20	1.08	0.70	0.43	0.68	0.82	0.21
	2	0.24	-134	-950	3.21	2.04	1.02	1.24	0.38	0.55	0.53	0.13
	3	0.10	-141	-970	4.33	2.65	1.30	1.51	0.38	0.42	0.52	0.41
12%	**1**	0.55	-138	-900	4.20	1.41	1.21	1.12	0.39	0.61	0.77	0.13
	2	0.50	-135	-944	4.69	2.04	1.38	1.44	0.33	0.51	0.55	0.09
	3	0.70	-136	-870	5.15	2.67	1.77	1.97	0.27	0.44	0.44	0.05
18%	**1**	1.06	-164	-900	4.25	1.43	1.31	1.44	0.39	0.62	0.94	0.24
	2	0.51	-147	-942	5.67	2.32	1.63	1.49	0.34	0.48	0.47	0.08
	3	1.04	-149	-850	6.06	2.88	1.89	2.23	0.28	0.42	0.34	0.04
21%	**1**	1.38	-183	-845	5.75	1.53	1.95	1.53	0.33	0.57	0.85	0.19
	2	1.17	-175	-910	6.16	2.96	1.66	1.53	0.36	0.42	0.48	0.42
	3	1.34	-191	-810	6.15	2.95	1.94	2.48	0.24	0.41	0.37	0.02

290

291 **TABLE 6**: Corrosion and film semiconductor data for as-received 316LN bars tested in pore
292 solution, with the N_x and d_x values defined in Figure 2.

Chloride addition		Electronic properties										
		i_{CORR} (mA/m^2)	E_{CORR} (mV$_{SCE}$)	E_{FB} (mV$_{SCE}$)	N_1 (10^{21} cm^{-3})	N_2 (10^{21} cm^{-3})	N_3 (10^{21} cm^{-3})	N_4 (10^{21} cm^{-3})	d_1 (nm)	d_2 (nm)	d_3 (nm)	d_4 (nm)
0%	**1**	0.01	-148	-920	3.54	2.03	1.37	0.84	0.34	0.50	0.47	0.08

	2	0.01	-161	-1010	5.69	2.62	1.56	1.78	0.34	0.45	0.42	0.13
	3	0.02	-138	-990	4.17	2.21	1.35	1.64	0.36	0.48	0.43	0.12
6%	**1**	0.04	-160	-900	6.39	3.26	2.18	1.76	0.25	0.40	0.46	0.09
	2	0.05	-174	-980	6.28	3.69	2.10	2.62	0.27	0.38	0.34	0.08
	3	0.07	-144	-980	6.29	3.38	2.03	2.43	0.27	0.39	0.35	0.07
12%	**1**	0.55	-166	-870	7.19	4.29	2.42	2.24	0.21	0.34	0.40	0.04
	2	0.25	-201	-970	7.87	4.5	2.45	2.95	0.25	0.35	0.33	0.10
	3	0.53	-152	-950	6.96	4.25	2.39	2.94	0.25	0.35	0.32	0.08
18%	**1**	0.81	-169	-860	7.82	5.07	3.16	3.15	0.19	0.31	0.32	0.01
	2	0.70	-224	-962	8.13	5.03	2.84	3.95	0.22	0.31	0.28	0.05
	3	0.65	-208	-950	8.05	4.89	2.67	3.82	0.22	0.32	0.28	0.04
21%	**1**	1.43	-216	-850	9.15	5.09	3.57	3.17	0.19	0.31	0.34	0.02
	2	1.74	-224	-955	8.44	5.19	3.59	4.02	0.22	0.32	0.28	0.04
	3	1.90	-278	-940	8.39	5.12	3.46	4.22	0.22	0.41	0.26	0.03

TABLE 7: Corrosion and film semiconductor data for as-received 24100 bars tested in pore solution, with the N_x and d_x values defined in Figure 2.

Chloride addition		**Electronic properties**										
		i_{CORR} (mA/m^2)	E_{CORR} (mV_{SCE})	E_{FB} (mV_{SCE})	N_1 (10^{21} cm^{-3})	N_2 (10^{21} cm^{-3})	N_3 (10^{21} cm^{-3})	N_4 (10^{21} cm^{-3})	d_1 (nm)	d_2 (nm)	d_3 (nm)	d_4 (nm)
0%	**1**	0.03	-155	-1031		1.21	1.28		0.45	0.59	0.65	
	2	0.02	-149	-1111	1.98	2.42	1.83	1.34	0.35	0.47	0.55	0.17
	3	0.03	-134	-1100	2.18	2.75	2.00	1.47	0.32	0.44	0.52	0.16
6%	**1**	0.11	-203	-988		1.47	1.31		0.37	0.53	0.68	
	2	0.21	-180	-1067	1.99	3.27	2.02	1.41	0.33	0.42	0.53	0.15
	3	0.20	-170	-1096	2.00	3.57	2.19	1.70	0.30	0.39	0.48	0.13
12%	**1**	0.36	-219	-980		1.61	1.62		0.32	0.45	0.59	
	2	0.48	-228	-1060	2.12	4.02	2.67	1.79	0.29	0.37	0.46	0.11

	3	0.42	-239	-1050	2.05	4.31	2.74	2.19	0.27	0.34	0.42	0.09
18%	**1**	1.05	-223	-971		2.52	1.76		0.27	0.41	0.52	
	2	1.19	-244	-1063	2.17	4.13	2.80	1.91	0.27	0.36	0.45	0.11
	3	1.41	-248	-1040	2.16	4.53	2.90	2.19	0.27	0.35	0.42	0.10
21%	**1**	2.33	-233	-970		2.96	1.88		0.26	0.43	0.48	
	2	2.91	-256	-1040	2.56	4.66	3.08	2.15	0.26	0.34	0.42	0.10
	3	3.50	-253	-1030	2.48	4.82	3.07	2.43	0.26	0.31	0.40	0.09

TABLE 8: Corrosion and film semiconductor data for as-received 2304 bars tested in pore solution, with the N_x and d_x values defined in Figure 2.

Chloride addition		**Electronic properties**										
		i_{CORR} (mA/m^2)	E_{CORR} (mV_{SCE})	E_{FB} (mV_{SCE})	N_1 (10^{21} cm^{-3})	N_2 (10^{21} cm^{-3})	N_3 (10^{21} cm^{-3})	N_4 (10^{21} cm^{-3})	d_1 (nm)	d_2 (nm)	d_3 (nm)	d_4 (nm)
0%	**1**	0.03	-104	-880		5.97	2.65		0.26	0.41	0.46	
	2	0.02	-83	-1070	10.40	6.44	3.99	7.51	0.22	0.29	0.20	0.04
	3	0.05	-79	-990	8.83	7.44	3.89	8.74	0.20	0.27	0.18	0.04
6%	**1**	0.12	-169	-860		6.49	3.87		0.24	0.39	0.38	
	2	0.08	-152	-997	10.11	8.73	5.05	7.66	0.18	0.23	0.19	0.03
	3	0.13	-145	-970	11.64	9.66	4.67	9.40	0.16	0.22	0.17	0.03
12%	**1**	0.70	-182	-850		8.63	4.98		0.22	0.37	0.37	
	2	0.55	-171	-990	10.08	11.65	5.51	8.37	0.16	0.21	0.18	0.02
	3	0.80	-166	-960	10.59	12.00	5.37	9.65	0.15	0.20	0.17	0.02
18%	**1**	0.91	-198	-861		9.80	5.29		0.21	0.36	0.35	
	2	1.20	-193	-992	10.98	13.08	6.17	8.66	0.15	0.19	0.15	0.01
	3	1.07	-188	-960	11.41	13.21	6.29	11.21	0.14	0.18	0.13	0.01
21%	**1**	2.14	-242	-840		10.95	6.47	1.22	0.16	0.33	0.29	0.06
	2	2.63	-266	-970	10.91	14.75	6.76	9.60	0.13	0.18	0.15	0.01
	3	2.90	-221	-920	13.41	15.24	7.18	13.63	0.12	0.17	0.13	0.00

299

300 **TABLE 9**: Corrosion and film semiconductor data for as-received 2205 bars tested in pore
301 solution, with the N_x and d_x values defined in Figure 2.

Chloride addition		Electronic properties										
		i_{CORR} (mA/m^2)	E_{CORR} (mV$_{SCE}$)	E_{FB} (mV$_{SCE}$)	N_1 (10^{21} cm^{-3})	N_2 (10^{21} cm^{-3})	N_3 (10^{21} cm^{-3})	N_4 (10^{21} cm^{-3})	d_1 (nm)	d_2 (nm)	d_3 (nm)	d_4 (nm)
0%	**1**	0.04	-139	-1121	7.32	3.94	2.43	3.32	0.20	0.38	0.37	0.49
	2	0.02	-147	-1120	9.25	5.35	2.96	4.00	0.25	0.32	0.28	0.83
	3	0.03	-147	-1140	7.91	4.52	2.52	3.22	0.30	0.37	0.36	0.65
6%	**1**	0.11	-191	-1067	13.37	9.38	4.80	7.06	0.16	0.23	0.22	0.17
	2	0.06	-167	-1070	9.89	5.67	3.24	4.31	0.24	0.31	0.27	0.18
	3	0.06	-180	-1059	9.42	7.71	3.66	5.23	0.21	0.28	0.29	0.15
12%	**1**	0.38	-202	-1022	13.48	9.72	6.08	7.12	0.17	0.22	0.23	0.14
	2	0.31	-183	-1010	10.77	9.06	3.76	5.11	0.26	0.31	0.37	0.13
	3	0.32	-207	-1050	11.47	9.72	4.58	6.21	0.18	0.23	0.21	0.12
18%	**1**	0.41	-216	-1005	15.72	9.98	6.26	7.26	0.17	0.23	0.23	0.14
	2	1.15	-227	-970	12.73	10.63	4.44	6.08	0.17	0.24	0.24	0.15
	3	0.51	-209	-1040	14.48	10.65	4.73	6.51	0.17	0.23	0.23	0.15
21%	**1**	2.56	-273	-1001	19.44	10.24	6.59	7.62	0.17	0.23	0.24	0.14
	2	3.98	-240	-880	15.35	11.12	4.93	7.07	0.17	0.22	0.20	0.16
	3	2.50	-273	-1030	15.53	11.30	5.41	7.60	0.18	0.23	0.23	0.16

302

303 **TABLE 10**: Corrosion and film semiconductor data for as-received carbon steel bars tested in
304 pore solution, with the N_x and d_x values defined in Figure 2.

Chloride addition	Electronic properties										
	i_{CORR} (mA/m^2)	E_{CORR} (mV$_{SCE}$)	E_{FB} (mV$_{SCE}$)	N_1	N_2 (10^{21} cm^{-3})	N_3 (10^{21} cm^{-3})	N_4 (10^{21} cm^{-3})	d_1	d_2 (nm)	d_3 (nm)	d_4 (nm)

0%	**1**	0.19	-161	-694		56	15	7		0.06	0.18	0.022
	2	0.28	-143	-637		67	20	9		0.06	0.11	0.083
	3	0.22	-159	-613		25	13	5		0.11	0.20	0.139
0.6%	**1**	1.01	-170	-710		183	98	34		0.04	0.07	0.025
	2	1.10	-181	-651		328	153	53		0.01	0.04	0.011
	3	1.03	-192	-624		295	132	41		0.02	0.05	0.017
1.2%	**1**	1.39	-252	-713		665	295	99		0.01	0.03	0.004
	2	2.50	-280	-707		551	299	89		0.02	0.04	0.009
	3	2.20	-311	-658		535	246	99		0.01	0.03	0.010
1.8%	**1**	2.4	-352	-701		675	268	103		0.01	0.03	0.006
	2	3.1	-341	-710		771	215	111		0.03	0.04	0.035
	3	3.3	-324	-676		711	321	112		0.01	0.03	0.006
2.4%	**1**	5.2	-391	-704		918	456	145		0.01	0.03	0.004
	2	4.2	-381	-680		1379	551	194		0.00	0.02	0.002
	3	4.5	-367	-684		736	327	124		0.01	0.03	0.009

TABLE 11: Corrosion data and film semiconductor data for polished cross-sections of all stainless steel bars tested in pore solution, with the N_x and d_x values defined in Figure 2.

Chloride addition		**Electronic properties**										
		i_{CORR} (mA/m^2)	E_{CORR} (mV_{SCE})	E_{FB} (mV_{SCE})	N_1 (10^{21} cm^{-3})	N_2 (10^{21} cm^{-3})	N_3 (10^{21} cm^{-3})	N_4 (10^{21} cm^{-3})	d_1 (nm)	d_2 (nm)	d_3 (nm)	d_4 (nm)
304L	0%	0.02	-164	-950	2.15	2.03	0.98	0.71	0.58	0.77	0.69	0.48
	21%	1.01	-202	-910	3.21	2.22	1.19	1.16	0.53	0.70	0.61	0.44
316LN	0%	0.02	-169	-1220	2.76	2.71	1.89	0.99	0.60	0.78	0.76	0.41
	21%	0.98	-200	-1180	4.75	2.93	2.13	1.95	0.54	0.72	0.70	0.38
24100	0%	0.02	-177	-1140	3.38	2.40	1.36	0.78	0.58	0.63	0.64	0.39
	21%	1.20	-210	-1100	4.11	3.52	2.73	2.51	0.53	0.60	0.58	0.38
2304	0%	0.05	-185	-1070	4.49	3.92	2.87	1.69	0.58	0.58	0.60	0.41

	21%	1.64	-231	-1010	7.65	4.31	3.65	2.99	0.53	0.53	0.52	0.39
2205	0%	0.04	-187	-1060	4.63	4.10	3.01	2.23	0.44	0.57	0.54	0.33
	21%	1.72	-242	-1010	7.70	4.53	3.43	3.09	0.43	0.53	0.51	0.32

for corrosion initiation. The austenitic grades had consistently lower defect densities and higher film thicknesses at all chloride levels than the duplex grades. This is consistent with the austenitic grades exhibiting the slightly lower average corrosion current densities than those of the duplex grades. Furthermore, the defect densities of the austenitic grades increase only slightly with increase in chlorides, whereas those of the duplex grades significantly increased in the presence of chlorides.

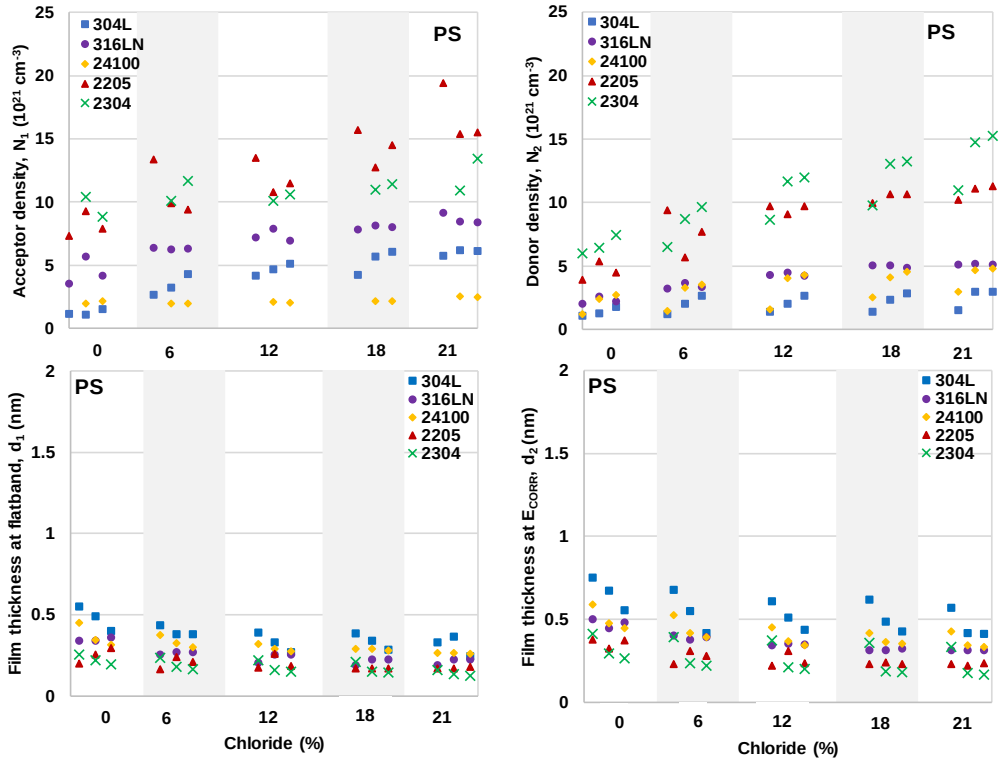

FIGURE 7. Change in acceptor and donor densities and film thicknesses at flatband and corrosion potentials for the stainless steel rebar with increasing chloride content in pore solutions.

Influence of alloying elements on electronic properties

Influence of chromium (Cr) in stainless steel bars on the electronic properties of the films.

As shown in Figure 5 and Tables 5 to 11, the influence of chromium was found both in the cathodic and anodic regions of the M-S plots and the defect densities associated with both regions. At very low cathodic potentials, the negative slope (indicative of a p-type semiconductor) not found in the carbon steel, reveals the inner Cr-rich oxide layer of the passive film. At more positive potentials, the plots of the carbon steel bars reveal a shallow (N_2) and deep (N_3) donor level, both characteristics of an n-type semiconductor, corresponding to Fe oxides in the space charge layer of the passive film. In the stainless bars, a positive sloped linear region, indicative of the outer Fe oxide in the passive film, was observed and, unlike the Cr-free carbon steel, a second acceptor level of the outer Fe-rich oxide layer exhibited a p-type semiconductor attributed to a Fe-Cr spinel. These findings agree with those of other authors who have tested Fe-Cr system [29], [30]. Tables 5 to 11 show that the defect densities, N_1 to N_4, and film thicknesses, d_1 to d_4, of the tested stainless steel bars are 1-2 orders of magnitude lower and higher, respectively, than those of the carbon steel bars with and without chlorides. This indicates that, although carbon steel does readily passivate at this high pH, the presence of Cr in the stainless steels promotes a more coherent, dense and thicker passive film.

Influence of nickel (Ni) in 304L and its replacement with manganese (Mn) in 24100 on the electronic properties of the films.

Due to the high cost of nickel (Ni) in the traditional 304L alloy, manganese (Mn) is used as an alternative austenite-promoting element in the production of the less costly 24100 grade. The effect can be assessed by comparing the electronic properties of both grades. Figure 7 show that the N_1 and N_2 values of the 24100 bars in pore solution with chlorides were lower and higher, respectively, than those of the 304L bars. The lower N_2 (also N_3 and N_4 shown in Tables 5 and 7) values of the 304L bars in the presence of chlorides suggest that the Ni-Fe oxides formed in the outer layer of the passive film of the 304L bars are denser and more coherent, and thus, offers more protection, than the possible Fe-Mn spinel formed in the passive films of the 24100 bars. From the lower and relatively constant N_1 values of the 24100, it is clear that the Mn stabilizes the inner Cr-rich oxide layers in the presence of chlorides. Some authors [13], [57] have also observed the influence of Ni only in the Fe-rich outer layer of the passive films.

Influence of molybdenum (Mo) in the austenitic and duplex stainless steel grades on the electronic properties of the films

The influence of molybdenum (Mo) on the electronic properties can be considered by comparing the pairs of the austenitic 304L and 316LN grades and the duplex 2205 and 2304 grades. The differences in two of the four defect densities (N_1, N_2) and film thicknesses (d_1, d_2) of both pairs of steels in solutions with and without chlorides can be graphically seen in Figure 7. The defect densities and film thicknesses of the Mo-containing bars, for both pairs of alloys are higher and lower, respectively, than those of their Mo-free counterparts.

In [10]–[13], the difference in semiconducting properties of traditional 304L and 316LN alloys was observed in the linear region of the M-S plot in potential range corresponding to those between potentials of -0.15 – +0.1 V, region for which defect densities N_3 were calculated, in this work. The authors found slightly lower defect densities for the 304L grade which is consistent with the data presented in the present work. No reference was found for which the electronic properties of both 2205 and 2304 steel grade had been assessed in the same work. The lower defect densities and higher film thicknesses of the 304L and 2304 bars than the 316LN and 2205 bars shown in Figure 7 and Tables 5, 6, 8 and 9 are consistent with their electrochemical properties in Figure 4.

Molybdenum is known to have a beneficial influence on the pitting resistance of stainless steels in acidic and neutral chloride solutions [58]. However, the corrosion potentials and corrosion current densities shown in Figures 4 do not show any improvement in corrosion resistance of 316LN over that or 304L, nor of 2205 over 2304. These results are in agreement with the findings of Mesquita et al. [59]–[61] who have shown that the beneficial effect of Mo in austenitic stainless alloys decreased with increasing pH from 0.6 to 7 to 10, at which level, its effect was negligible. For the duplex alloys, on the other hand, Mesquita et al. [59]–[61] and Cheng et al. [31]–[33] showed that the Mo and Cr were partitioned preferentially in the ferrite phase and that the positive influence of Mo diminished only slightly with increasing pH in 2205. Moreover, these authors found the ferrite and austenite acted synergistically in the 2205 to provide corrosion protection by promoting the formation of a denser and more homogeneous passive film. This provides an explanation for the superior corrosion resistance of 2205 grade compared with both

2304 and 316LN observed in previous work [62]. However, in the present work, 2205 did not perform as well as expected. Therefore, some of the untested bars of the 2205 specimens were sectioned, polished and observed by optical microscopy. It was found that the surface of these bars was heavily pitted on a micro-scale, as shown in Figure 8. It is believed that this is a result of the pickling process mentioned earlier and that it has allowed an increased level of corrosion to occur in the current tests. This surface pitting explains why there is more scatter in the corrosion current densities, shown in Figure 4, of the 2205 bars than of other rebar grades.

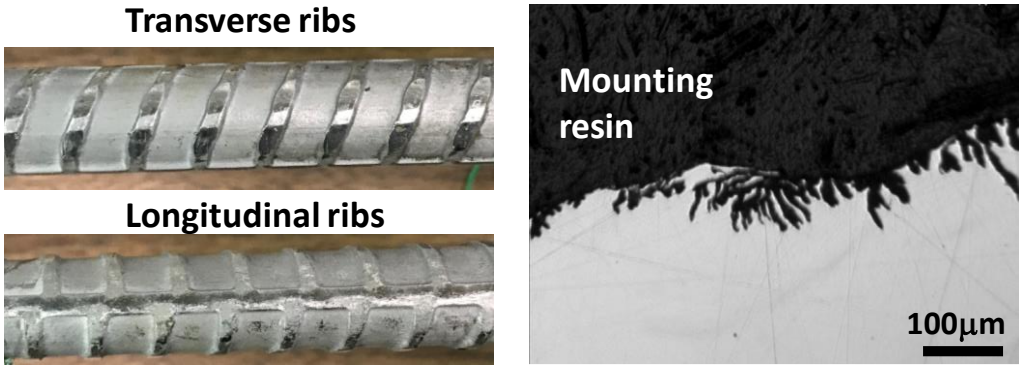

FIGURE 8. Sample of the 2205 stainless steel rebar showing the transverse and longitudinal ribs (left) and the image of the cross section showing micropits on the longitudinal rib (right)

In order to correlate the electronic and electrochemical corrosion data, the Mott-Schottky (M-S) curves and corresponding cyclic polarization (CP) curves for 304L and 316LN and for the 2304 and 2205 bars tested 0% and 6% Cl^- solutions are shown in Figures 9 and 10 respectively.

The information provided by Hakiki et al. [10]–[13] and Beverskog & Puigdomenech [63]–[65] are considered in interpreting these graphs, which have been labelled to reflect the state of the passive film in the different regions of the M-S and cyclic polarization plots. The flatband potential of the M-S plots of the stainless steel bars presented in Figures 9 and 10 corresponds approximately to the H^+/H_2 equilibrium potential. The highest peak in the M-S plots corresponds to the corrosion potentials and, the onset of the transpassive region corresponds to the O_2/OH^- equilibrium potential on the E/pH diagram at the pH of the pore solution. The slight shift in potentials between the M-S and the CP plots is attributed to the difference in scan rates of the two tests.

The plots shown in Figures 9 and 10 indicate that, on raising the potential in the anodic direction from -1.50 V_{SCE}, the p-type semiconducting Cr-rich oxide films become more unstable and, at potentials more positive than the flatband potential, the M-S curve is dominated by an n-type Fe_2O_3 and/or the spinel $FeCr_2O_4$ films. At potential more positive than the corrosion potential of the material, there is an oxidation of the spinel $FeCr_2O_4$ to $(Fe)CrO_4^{2-}$ until the stable $NiFe_2O_4$ spinel is formed. At even more positive potentials, there is transpassive oxidation back to CrO_4^{2-} and FeO_4^{2-}. The last potential range (~ +0.3 – +0.6 VSCE) on the M-S plots for which the N4 defect densities were calculated is interpreted to be the transpassive region as per their CP plots. Williamson and Isgor [26], used the inversion layer theory of Morrison [36] to explain this characteristic transition in carbon steel rebar to a p-type behaviour. They interpreted the transition as being due to exhaustion of the two distinct donor layers within the band gap (N_2 and N_3 values in the present study), thus requiring transfer of charge from the valence band and further conduction by holes, i.e. p-type conduction. Nevertheless, for both stainless steel and carbon steel in the present study, this p-type behaviour results in the M-S curve approaching zero corresponding to the sharp increase in current density of the cyclic polarization curve, i.e. equivalent to transpassive behaviour. The interpretation made in the present study regarding oxide species formed at the different potentials agrees well with the E/pH diagrams in [63]–[65] and observations from M-S analysis by other authors [5], [10]–[13], [27]–[33].

With respect to the influence of Mo, the corrosion current densities of the Mo-free 304L bars are lower than those of the Mo-containing 316LN grades and, as discussed, the expected superior behaviour of the Mo-containing 316LN was not observed. At 6% chloride additions, the corrosion potentials of the 316LN bars became more negative; a behaviour not observed in the 304L bars. These findings support other authors' observation [31]–[33], [59]–[61],[66] that the influence of Mo in austenitic phase diminishes with pH. On the other hand, both the corrosion current densities of the Mo-containing 2205 grades and the intensity of the peak attributed to the $FeCr_2O_4$ oxidation are lower than those of the Mo-free 2304 grades. However, after the addition of chlorides, the $FeCr_2O_4$ oxidation peak was higher in the 2205 bars due to the heavy pitting observed around the bars. These findings are also consistent with those from other authors [31]–[33], [59]–[61],[66] who observed Mo to be beneficial in the ferritic phases of the duplex alloys.

The overall observation in Figure 9 and 10 is consistent with previous data presented on corrosion potential, corrosion current density, defect densities and film thicknesses.

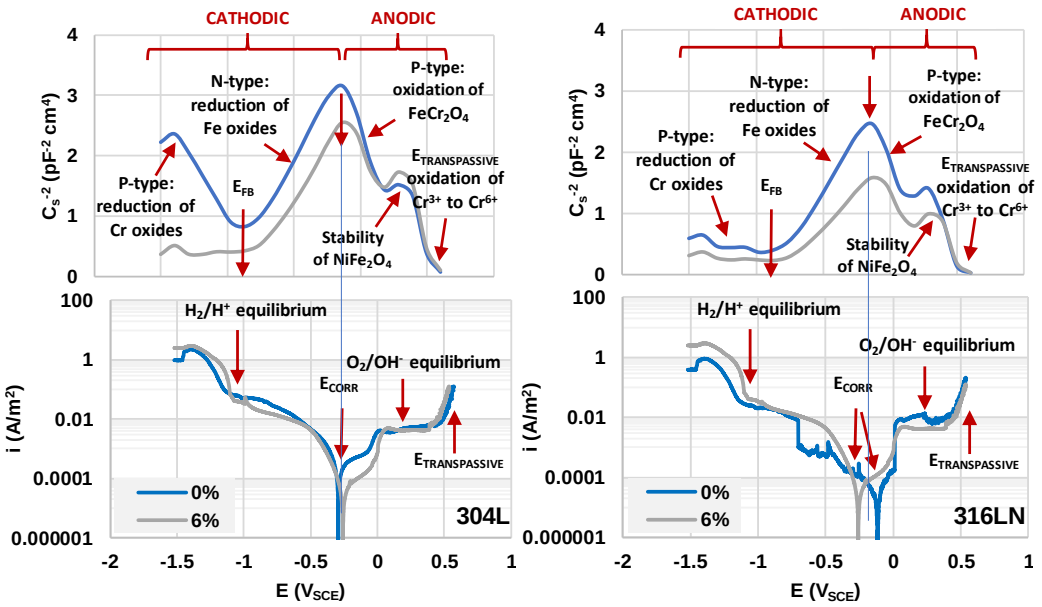

FIGURE 9. Mott-Schottky and cyclic polarization curves for 304L and 316LN stainless steel bars in solution without and with 6% chlorides. Test were carried out with similar potential range. Note that the plots are shifted slightly to align the corrosion potentials, to account for the different scan rates and specimens employed for the two tests.

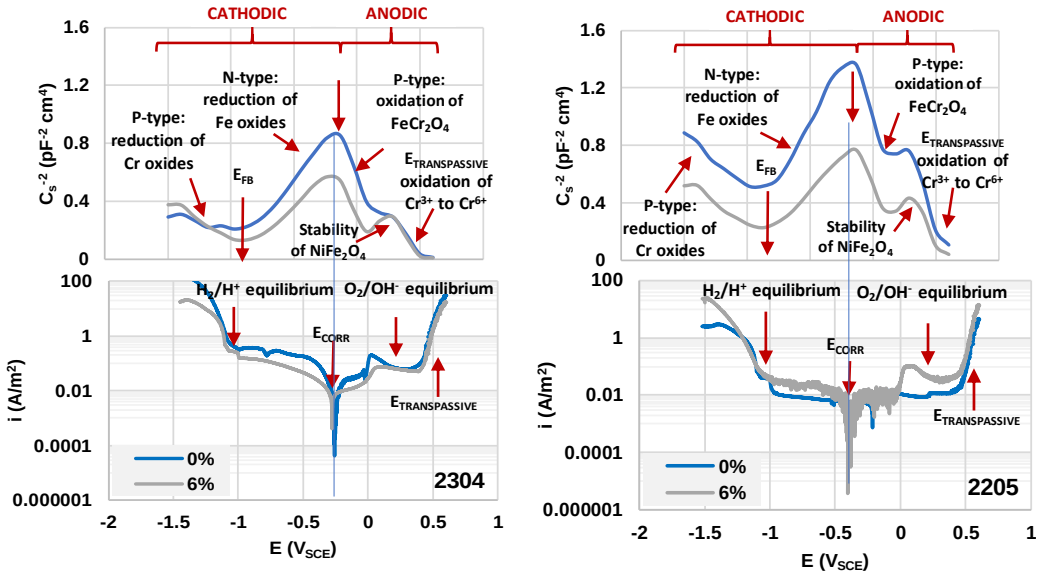

FIGURE 10. Mott-Schottky and cyclic polarization curves for 2304 and 2205 stainless steel bars in solution without and with 6% chlorides. Test were carried out with similar potential range. Note that the plots are shifted slightly to align the corrosion potentials, to account for the different scan rates and specimens employed for the two tests.

Breakdown of passive film by chlorides

An interesting observation in the CP and M-S plots of the 304L bars shown in Figure 9 is that there is little effect of 6% Cl- on the polarization curve, while there is a significant drop in the slope attributed to the Cr-rich component of the film in the cathodic region of the M-S plot. This can also be observed in the defect densities presented in Tables 5 – 9 and 11 for both as-received and polished cross-section where the N_1 values are generally higher than the N_2 and N_3 values. This is surprising in view of the fact the N_1 represents the defects in the inner layer of the film and there appears to be little effect on the outer Fe-rich layer. A possible explanation to this observation can be explained considering the film breakdown.

Most models of chloride-induced corrosion of reinforcing steels include an incubation period in which both the corrosion potential, E_{corr}, and passive corrosion current density, $i_{corr,}$ are approximately constant. When sufficient chloride is present at the steel surface to breakdown the passive film and initiate active corrosion (the so-called threshold value), the models predict a sharp increase in i_{corr} accompanied by a shift in E_{corr} to more negative values. In practice, this is not what happens. As illustrated in Figure 4 for both carbon steel and stainless steel rebar, there is a gradual increase in i_{corr} and decrease in E_{corr} with increasing chloride content of the solution, requiring a very different model of the process. The model of Marcus et al. [67], shown schematically in Figure 11, can provide a basis for such a model.

Marcus and colleagues propose that there is a sharp potential difference, ΔE, at the interface between the metal and the passive film and another at the interface between the film and the solution, with a gradual potential gradient across the film. Increasing the defects in the film by, for example, diffusion of chloride ions, allows for reduced electronic and ionic resistance and thinning of the film. Such a process would result in a greater leakage current and a more negative potential difference. This model can be coupled with that of Hakiki et al. [12] shown in Figure 12 in which Cl^- diffuses through the oxygen vacancies of the Fe-rich layer and reacts with the Fe^{2+} ions diffusing outwards through the Cr-rich layer. This would explain the significant effect of 6% chloride on the inner Cr-rich layer of 304L with little effect on the Fe-rich layer, observed by M-S analysis and little effect on the measured cyclic polarization curves Figure 9.

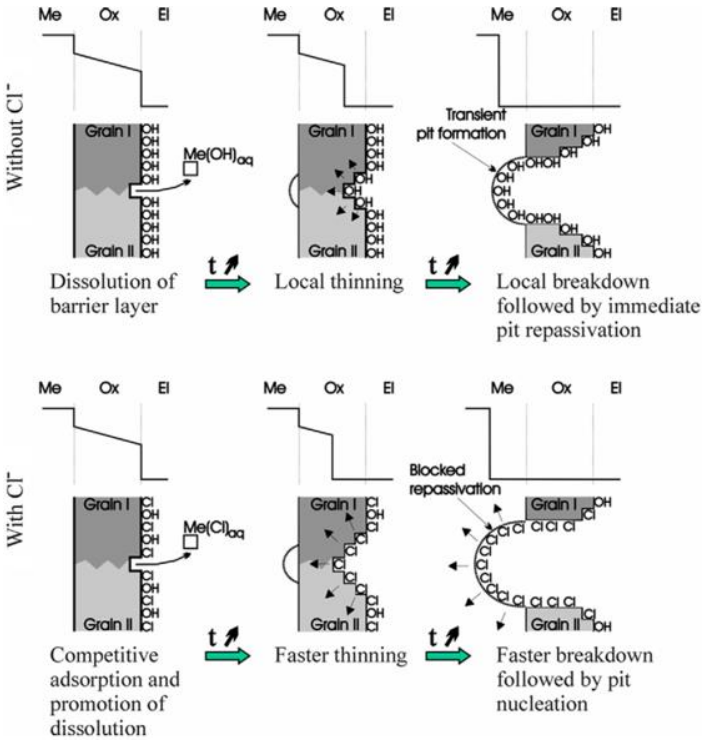

FIGURE 11. Mechanism of local breakdown of passivity driven by the potential drop at the oxide/electrolyte interface of an inter-granular boundary of the barrier layer. The effect of chlorides is shown [67].

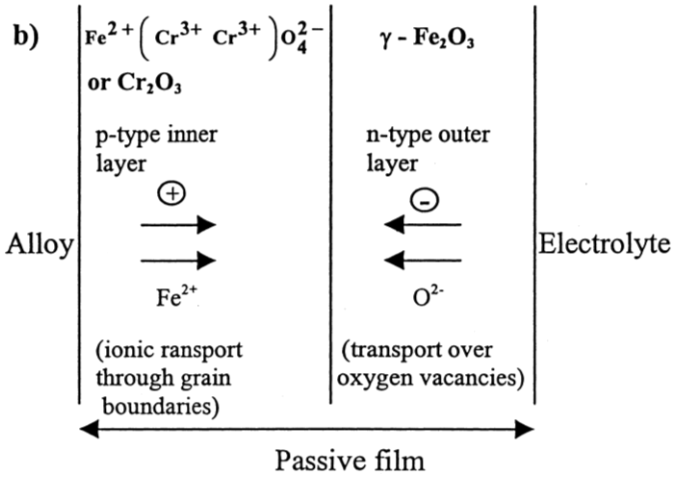

FIGURE 12. Schematic representation of the diffusion processes through the individual layers of passive films [12].

Influence of surface finish on electronic properties

From Tables 5 – 9 and 11, the defect densities obtained from the polished cross-section specimens are similar to those from the as-received austenitic stainless steel grades and, significantly lower than those from the as-received duplex grades, suggesting that the passive films formed on the polished cross-sections were more protective in the presence of chlorides. Apart from the larger surface area available for chlorides to attack in the as-received bars, the surface roughness of the bars (an example for which is shown in Figure 8) being attacked by chlorides contributes to the higher defect density values. This is also supported by the slightly more negative E_{CORR} and higher i_{CORR} values at 21% chlorides shown in Table 11 than those in Tables 5 - 10.

Similar to the trend found in the as-received bars, the defect densities from the polished cross-sections of the duplex stainless steel alloys are also higher than those of the austenitic grades. Similar results, in most cases, obtained in both polished cross-sections and the as-received bars suggest that the relative performance of bars to be compared can be tested in their as-received conditions, without polishing their cross-sections. However, in other cases, the impact of chlorides once added to the testing solution of the duplex stainless steel cross-sections, can be underestimated, emphasising the importance of replicating test conditions found in the field.

SUMMARY AND CONCLUSIONS

- The positive impact of the chromium in the stainless steel bars is attributed to the significantly lower defect densities, by 1 – 2 orders of magnitude, of their passive film than that of the carbon steel bars.
- Molybdenum, which is the major difference in composition between austenitic 304L and 316LN and the duplex 2205 and 2304, did not show the anticipated positive impact on the electrochemical and electronic properties of the 316LN and 2205 alloys in all testing solutions with and without chlorides.
- On comparing the data for the 304L and 24100 bars to evaluate the influence of replacing Ni with Mn, manganese was found to reduce the defect density of the inner Cr-rich oxide layer while nickel decreased that of the outer Fe-rich oxides. In general, the electronic

properties and electrochemical behaviour of the Ni-containing 304L bars were not significantly superior than those of the Mn-containing 24100 bars.

- The roughness, on both macro- and micro-scale, of the as-received surface of the bars did not influence the shape of the M-S plots, but their passive films had a higher defect density than those of the polished surface. Consequently, M-S analysis can be performed on as-received bars, although great amount of scatter may be obtained.
- Increasing additions of chlorides to the solution made the passive films on all tested bars more defective and reduced their thicknesses, resulting in a gradual increase in the passive current densities accompanied by a more negative corrosion potential.
- For the stainless steels, the M-S analysis indicates that the chlorides affect the Cr-rich inner layer of the passive film more than the Fe-rich outer layer.
- The electronic properties of the passive films on the three austenitic stainless steel grades tested did not vary significantly with chlorides, whereas those of the duplex grades changed significantly in the presence of chlorides. This observation is consistent with the higher corrosion rate and more negative corrosion potential values of the duplex stainless steel grades.

Acknowledgments

The authors appreciate the funding provided by the Natural Sciences and Engineering Research Council of Canada (NSERC) and donations of steel from Valbruna and North American Stainless.

Declaration of Interest: None

References

[1] P. Ghods, O. B. Isgor, J. R. Brown, F. Bensebaa, and D. Kingston, "XPS depth profiling study on the passive oxide film of carbon steel in saturated calcium hydroxide solution and the effect of chloride on the film properties," *Appl. Surf. Sci.*, vol. 257, no. 10, pp. 4669–4677, 2011.

[2] P. Ghods, O. Burkan Isgor, F. Bensebaa, and D. Kingston, "Angle-resolved XPS study of carbon steel passivity and chloride-induced depassivation in simulated concrete pore

solution," *Corros. Sci.*, vol. 58, pp. 159–167, 2012.

[3] H. B. Gunay, P. Ghods, O. B. Isgor, G. J. C. Carpenter, and X. Wu, "Characterization of atomic structure of oxide films on carbon steel in simulated concrete pore solutions using EELS," *Appl. Surf. Sci.*, vol. 274, pp. 195–202, 2013.

[4] H. Schmuki, P., Bohni, "Metastable Pitting and Semiconductive Properties of Passive films," *J. Electrochem. Soc.*, vol. 139, no. 7, pp. 1908–1913, 1992.

[5] A. Simoes, M. Ferreira, B. Rondot, and M. Da Cunha Belo, "Study of passive films on AISI 304 Stainless steel by impedance measurement and photoelectrochemistry," *J. Electrochem. Soc.*, vol. 137, no. 1, pp. 82–87, 1990.

[6] A. Di Paola, F. Di Quarto, and C. Sunseri, "Photochemical characterization of passive films on stainless steels," *Corros. Sci.*, vol. 26, no. 11, pp. 935–948, 1986.

[7] I. Díez-Pérez, P. Gorostiza, and F. Sanz, "Direct Evidence of the Electronic Conduction of the Passive Film on Iron by EC-STM," *J. Electrochem. Soc.*, vol. 150, no. 7, p. B348, 2003.

[8] I. Dıez-Perez, A. G. Guell, F. Sanz, and P. Gorostiza, "Conductance Maps by Electrochemical Tunneling Spectroscopy To Fingerprint the Electrode Electronic Structure," *Anal. Chem.*, vol. 78, no. 20, pp. 7325–7329, 2006.

[9] M. D. Porter, T. B. Bright, D. L. Allara, and C. E. D. Chidsey, "Spontaneously organized molecular assemblies. 4. Structural characterization of n-alkyl thiol monolayers on gold by optical ellipsometry, infrared spectroscopy, and electrochemistry," *J. Am. Chem. Soc.*, vol. 109, no. 12, pp. 3559–3568, Jun. 1987.

[10] M. F. Montemor, M. G. S. Ferreira, N. E. Hakiki, and M. Da Cunha Belo, "Chemical composition and electronic structure of the oxide films formed on 316L stainless steel and nickel based alloys in high temperature aqueous environments," *Corros. Sci.*, vol. 42, no. 9, pp. 1635–1650, 2000.

[11] N. E. Hakiki, S. Boudin, B. Rondot, and M. Da Cunha Belo, "The electronic structure of passive films formed on stainless steels," *Corros. Sci.*, vol. 37, no. 11, pp. 1809–1822, 1995.

[12] N. E. Hakiki, M. F. Montemor, M. G. S. Ferreira, and M. da Cunha Belo, "Semiconducting properties of thermally grown oxide films on AISI 304 stainless steel," *Corros. Sci.*, vol. 42, no. 4, pp. 687–702, 2000.

[13] N. E. Hakiki, M. Da Cunha Belo, A. M. P. Simoẽs, and M. G. S. Ferreira, "Semiconducting properties of passive films formed on stainless steels: Influence of the alloying elements,"

564 *J. Electrochem. Soc.*, vol. 145, no. 11, pp. 3821–3829, 1998.
565 [14] N. Sato, "An overview on the passivity of metal," *Corros. Sci.*, vol. 31, pp. 1–19, 1990.
566 [15] U. Stimming and J. W. Schultze, "A semiconductor model of the passive layer on iron
567 electrodes and its application to electrochemical reactions," *Electrochim. Acta*, vol. 24, no.
568 8, pp. 859–869, 1979.
569 [16] M. H. Dean and U. Stimming, "Capacity of semiconductor electrodes with multiple bulk
570 electronic states Part I. Model and calculations for discrete states," *J. Electroanal. Chem.*,
571 vol. 228, no. 1–2, pp. 135–151, 1987.
572 [17] N. F. Mott, "The theory of crystal rectifiers," *R. Soc. London*, vol. 171, no. Series A, pp.
573 27–38, 1939.
574 [18] W. Schottky, "Zur Halbleitertheorie der Sperrschicht- und Spitzengleichrichter," *Nat. Sci.*,
575 vol. 26, no. 843, pp. 1432–1904, 1938.
576 [19] M. Sánchez, J. Gregori, M. C. Alonso, J. J. García-Jareño, and F. Vicente, "Anodic growth
577 of passive layers on steel rebars in an alkaline medium simulating the concrete pores,"
578 *Electrochim. Acta*, vol. 52, no. 1, pp. 47–53, 2006.
579 [20] M. Sánchez, J. Gregori, C. Alonso, J. J. García-Jareño, H. Takenouti, and F. Vicente,
580 "Electrochemical impedance spectroscopy for studying passive layers on steel rebars
581 immersed in alkaline solutions simulating concrete pores," *Electrochim. Acta*, vol. 52, no.
582 27 SPEC. ISS., pp. 7634–7641, 2007.
583 [21] Y. Zhang and Q. Li, "Electrochemical study on semiconductive properties of the passive
584 film on rebar in concrete," *J. Zhejiang Univ. Sci. A*, vol. 7, no. 8, pp. 1447–1452, 2006.
585 [22] L. Hamadou, A. Kadri, and N. Benbrahim, "Characterisation of passive films formed on
586 low carbon steel in borate buffer solution (pH 9.2) by electrochemical impedance
587 spectroscopy," *Appl. Surf. Sci.*, vol. 252, no. 5, pp. 1510–1519, 2005.
588 [23] Y. F. Cheng and J. L. Luo, "Passivity and pitting of carbon steel in chromate solutions,"
589 *Electrochim. Acta*, vol. 44, no. 26, pp. 4795–4804, 1999.
590 [24] D. G. Li, Y. R. Feng, Z. Q. Bai, J. W. Zhu, and M. S. Zheng, "Influence of temperature,
591 chloride ions and chromium element on the electronic property of passive film formed on
592 carbon steel in bicarbonate/carbonate buffer solution," *Electrochim. Acta*, vol. 52, no. 28,
593 pp. 7877–7884, 2007.
594 [25] Y. Zhang and A. Poursaee, "Study of the semi-conductive behavior of the passive film on

carbon steel in simulated concrete pore solution under stress," *Anti-Corrosion Methods Mater.*, vol. 62, no. 6, pp. 363–370, 2015.

[26] J. Williamson and O. B. Isgor, "The effect of simulated concrete pore solution composition and chlorides on the electronic properties of passive films on carbon steel rebar," *Corros. Sci.*, vol. 106, pp. 82–95, 2016.

[27] J. J. Kim and Y. M. Young, "Study on the passive film of type 316 stainless steel," *Int. J. Electrochem. Sci.*, vol. 8, no. 10, pp. 11847–11859, 2013.

[28] Z. Feng, X. Cheng, C. Dong, L. Xu, and X. Li, "Effects of dissolved oxygen on electrochemical and semiconductor properties of 316L stainless steel," *J. Nucl. Mater.*, vol. 407, no. 3, pp. 171–177, 2010.

[29] I. H. Toor, M. Ejaz, and H. S. Kwon, "Mott–Schottky analysis of passive films on Cu containing Fe–20Cr–xCu (x=50, 4) alloys," *Corrison Eng. Sci. Technol.*, vol. 49, no. 5, pp. 1–6, 2014.

[30] I. Toor, "Mott-Schottky Analysis of Passive Films on Si Containing Stainless," *J. Electrochem. Soc.*, vol. 158, no. 11, pp. 391–395, 2011.

[31] H. Luo, C. F. Dong, X. G. Li, and K. Xiao, "The electrochemical behaviour of 2205 duplex stainless steel in alkaline solutions with different pH in the presence of chloride," *Electrochim. Acta*, vol. 64, pp. 211–220, 2012.

[32] H. Tian, X. Cheng, Y. Wang, C. Dong, and X. Li, "Effect of Mo on interaction between a/g phases of duplex stainless steel," *Electrochim. Acta*, vol. 267, pp. 255–268, 2018.

[33] X. Cheng, Y. Wang, C. Dong, and X. Li, "The beneficial galvanic effect of the constituent phases in 2205 duplex stainless steel on the passive films formed in a 3.5% NaCl solution," *Corros. Sci.*, vol. 134, pp. 122–130, 2018.

[34] A. W. Bott and D. Ph, "Electrochemistry of Semiconductors," *Sol. Energy*, vol. 8, no. 4, p. 136, 1964.

[35] J. F. Dewald, "The charge distribution at the zinc oxide-electrolyte interface," *J. Phys. Chem. Solids*, vol. 14, pp. 155–161, 1960.

[36] S. R. Morrison, *Electrochemistry at semiconductor and oxidized metal electrodes*. Springer, New York, USA, 1980.

[37] B. science Instrument, "EC-Lab Software : Techniques and Applications," *BioLogic*, vol. 10.37, no. February, 2011.

626 [38] A. J. Nozik, “Annual review of physical chemistry,” *Annu. Rev. Phys. Chem.*, vol. 29, pp.
627 189–222, 1978.
628 [39] D. D. Macdonald, “The Point Defect Model for the passive state,” *J. Electrochem. Soc.*, vol.
629 139, no. 12, p. 3434, 1992.
630 [40] J. Sikora, E. Sikora, and D. D. MacDonald, “Electronic structure of the passive film on
631 tungsten,” *Electrochim. Acta*, vol. 45, no. 12, pp. 1875–1883, 2000.
632 [41] D. D. Macdonald, “On the Existence of Our Metals-Based Civilization,” *J. Electrochem.*
633 *Soc.*, vol. 153, no. 7, p. B213, 2006.
634 [42] A. Goossens, M. Vazquez, and D. D. Macdonald, “The nature of electronic states in anodic
635 zirconium oxide films part 1: the potential distribution,” *Electrochim. Acta*, vol. 41, no. 1,
636 pp. 35–45, 1996.
637 [43] E. Sikora and D. D. Macdonald, “Nature of the passive film on nickel,” *Electrochim. Acta*,
638 vol. 48, no. 1, pp. 69–77, 2002.
639 [44] D. D. Macdonald, “Passivity–the key to our metals-based civilization,” *Pure Appl. Chem.*,
640 vol. 71, no. 6, pp. 951–978, 1999.
641 [45] E. Cho, H. Kwon, and D. D. Macdonald, “Photoelectrochemical analysis on the passive film
642 formed on Fe-20Cr in pH 8.5 buffer solution,” *Electrochim. Acta*, vol. 47, no. 10, pp. 1661–
643 1668, 2002.
644 [46] U. Stimming and J. Schultze, “No Title,” *Berichte der Bunsengesellschaft fur Phys. chemie*,
645 vol. 80, pp. 1297–1302, 1976.
646 [47] H. Wu, Y. Wang, Q. Zhong, M. Sheng, H. Du, and Z. Li, “The semi-conductor property
647 and corrosion resistance of passive film on electroplated Ni and Cu – Ni alloys,” *J.*
648 *Electroanal. Chem.*, vol. 663, no. 2, pp. 59–66, 2011.
649 [48] C. M. Hansson and T. D. Marcotte, “Corrosion products that form on steel within cement
650 paste,” *Mater. Struct.*, vol. 40, pp. 325–340, 2007.
651 [49] S. Randstrom, M. Almen, R. Pettersson, and M. Adair, “Reproducibility of critical chloride
652 threshold levels for stainless steel reinforcement,” in *Structural Faults*, 2010.
653 [50] C. B. Van Niejenhuis, I. G. Ogunsanya, and C. M. Hansson, “Analysis of pore solution
654 expressed from Portland cement pastes with and without supplementary cementitious
655 materials and admixed chlorides,” *ACI Mater. J.*, vol. submitted, 2018.
656 [51] L. Bertolini, F. Bolzoni, T. Pastore, and P. Pedeferri, “Behaviour of stainless steel in

simulated concrete pore solution," *Br. Corros. J.*, vol. 31, no. 3, pp. 218–222, 1996.

[52] L. Bertolini and M. Gastaldi, "Corrosion resistance of austenitic and low-nickel duplex stainless steel bars," in *Corrosion from the nanoscale to the plant*, 2009.

[53] M. F. Hurley and J. R. Scully, "Threshold chloride concentrations of selected corrosion-resistant rebar materials compared to carbon steel," *Corrosion*, vol. 62, no. 10, pp. 892–904, 2006.

[54] I. G. Ogunsanya and C. M. Hansson, "Detection of the critical chloride threshold of carbon steel rebar in synthetic concrete pore solutions," *RILEM Tech. Lett.*, vol. 3, pp. 75–83, 2018.

[55] M. Stern and A. L. Geary, "Electrochemical Polarization," *J. Electrochem. Soc.*, vol. 104, no. 9, p. 559, 1957.

[56] Kyle A. Anders, *The Effect of Surface and Loading Conditions on the Corrosion Performance of Stainless Steel Rebar*. 2009.

[57] E. Hamada, K. Yamada, M. Nagoshi, N. Makiishi, K. Sato, T. Ishii, K. Fukuda, S. Ishikawa, and T. Ujiro, "Direct imaging of native passive film on stainless steel by aberration corrected STEM," *Corros. Sci.*, vol. 52, no. 12, pp. 3851–3854, 2010.

[58] W. A. Badawy and F. M. Al-Kharafi, "Corrosion and passivation behaviors of molybdenum in aqueous solutions of different pH," *Electrochim. Acta*, vol. 44, no. 4, pp. 693–702, 1998.

[59] T. J. Mesquita, E. Chauveau, M. Mantel, N. Kinsman, and R. P. Nogueira, "Influence of Mo alloying on reinforcement steels used as concrete pitting corrosion of stainless," *Metall. Mater.*, vol. 66, no. 2, pp. 173–178, 2013.

[60] T. J. Mesquita, E. Chauveau, M. Mantel, N. Kinsman, and R. P. Nogueira, "Anomalous corrosion resistance behavior of Mo-containing SS in alkaline media: The role of microstructure," *Mater. Chem. Phys.*, vol. 126, no. 3, pp. 602–606, 2011.

[61] T. J. Mesquita, E. Chauveau, M. Mantel, and R. P. Nogueira, "A XPS study of the Mo effect on passivation behaviors for highly controlled stainless steels in neutral and alkaline conditions," *Appl. Surf. Sci.*, vol. 270, pp. 90–97, 2013.

[62] C. B. Van Niejenhuis, S. Walbridge, and C. M. Hansson, "The performance of austenitic and duplex stainless steels in cracked concrete exposed to concentrated chloride brine," *J. Mater. Sci.*, vol. 51, no. 1, pp. 362–374, 2016.

[63] B. Beverskog and I. Puigdomenech, "Revised Pourbaix diagrams for iron at 25-300°C," *Corros. Sci.*, vol. 38, no. 12, pp. 2121–2135, 1996.

[64] B. Beverskog and I. Puigdomenech, “Revised Pourbaix Diagrams for Cr at 25C-300C.pdf,” *Corros. Sci.*, vol. 39, no. 1, pp. 43–57, 1997.

[65] B. Beverskog and I. Puigdomenech, “Revised pourbaix diagrams for nickel at 25-300°C,” *Corros. Sci.*, vol. 39, no. 5, pp. 969–980, 1997.

[66] L. A. Shaik and S. K. Thamida, “Simulation of corrosion of a dual phase alloy steel based on its constituent phase polarization properties,” *Materialia*, vol. 2, pp. 183–189, 2018.

[67] P. Marcus, V. Maurice, and H. H. Strehblow, “Localized corrosion (pitting): A model of passivity breakdown including the role of the oxide layer nanostructure,” *Corros. Sci.*, vol. 50, no. 9, pp. 2698–2704, 2008.